J|A|C|S
ARTICLES
Published on Web 02/01/2008

Probing Chemical Shifts of Invisible States of Proteins with Relaxation Dispersion NMR Spectroscopy: How Well Can We Do?

D. Flemming Hansen, Pramodh Vallurupalli, Patrik Lundström, Philipp Neudecker, and Lewis E. Kay*

Departments of Medical Genetics, Biochemisty and Chemistry, University of Toronto, Toronto, Ontario, Canada, M5S 1A8

Received October 31, 2007; E-mail: kay@pound.med.utoronto.ca

Abstract: Carr−Purcell−Meiboom−Gill relaxation dispersion NMR spectroscopy has evolved into a powerful approach for the study of low populated, invisible conformations of biological molecules. One of the powerful features of the experiment is that chemical shift differences between the exchanging conformers can be obtained, providing structural information about invisible excited states. Through the development of new labeling approaches and NMR experiments it is now possible to measure backbone $^{13}C^{\alpha}$ and ^{13}CO relaxation dispersion profiles in proteins without complications from $^{13}C-^{13}C$ couplings. Such measurements are presented here, along with those that probe exchange using ^{15}N and ^{1}HN nuclei. A key experimental design has been the choice of an exchanging system where excited-state chemical shifts were known from independent measurement. Thus it is possible to evaluate quantitatively the accuracy of chemical shift differences obtained in dispersion experiments and to establish that in general very accurate values can be obtained. The experimental work is supplemented by computations that suggest that similarly accurate shifts can be measured in many cases for systems with exchange rates and populations that fall within the range of those that can be quantified by relaxation dispersion. The accuracy of the extracted chemical shifts opens up the possibility of obtaining quantitative structural information of invisible states of the sort that is now available from chemical shifts recorded on ground states of proteins.

Introduction

The analysis of nuclear spin relaxation rates can, in principle, provide a wealth of information about molecular dynamics over a range of time-scales, extending from picoseconds to seconds.[1−4] Moreover, because separate signals corresponding to individual probes are observed in NMR spectra it is possible to characterize the dynamics on a site-specific basis. On the basis of these strengths it is not surprising that a large number of multidimensional NMR relaxation experiments have been developed for studies of biomolecular dynamics and that results from such analyses are providing important links between motion and function.[3,5−7] One class of experiment that has gained in popularity in recent years[8,9] measures millisecond time-scale dynamics through the quantification of the linewidths of signals (transverse relaxation) as a function of the application of radio frequency pulses in a Carr−Purcell−Meiboom−Gill[10,11] (CPMG) spin−echo train. A particularly powerful feature of this so-called relaxation dispersion methodology is that it can be applied to exchanging systems involving a dominant NMR observable (ground) state interconverting with low-populated (excited) states that cannot be probed directly. The kinetics of such an exchange process can be quantified so long as the low-populated state(s) are present at a level of approximately 0.5% with exchange on the millisecond time-scale. The kinetic parameters, in turn, can be used to determine the energetics of the exchange process[12] and from measurements of the variation of kinetics with temperature it becomes possible to extract enthalpic and entropic contributions to the free energy.[12,13] Similarly, the pressure dependence of the kinetics can be used to derive changes in partial molar volumes and compressibilities between states that are along the exchange pathway.[14,15]

In addition to the thermodynamic parameters that can be obtained it is also possible to measure chemical shifts of low-

(1) Palmer, A. G.; Williams, J.; McDermott, A. *J. Phys. Chem.* **1996**, *100*, 13293−13310.
(2) Peng, J. W.; Wagner, G. *Methods Enzymol.* **1994**, *239*, 563−596.
(3) Ishima, R.; Torchia, D. A. *Nat. Struct. Biol.* **2000**, *7*, 740−743.
(4) Mittermaier, A.; Kay, L. E. *Science* **2006**, *312*, 224−228.
(5) Wagner, G. *Nat. Struct. Biol.* **1997**, (Suppl. 4), 841−844.
(6) Kay, L. E. *Nat. Struct. Biol. NMR Suppl.* **1998**, *5*, 513−516.
(7) Boehr, D. D.; Dyson, H. J.; Wright, P. E. *Chem. Rev.* **2006**, *106*, 3055−3079.
(8) Palmer, A. G.; Grey, M. J.; Wang, C. *Methods Enzymol.* **2005**, *394*, 430−465.
(9) Palmer, A. G.; Kroenke, C. D.; Loria, J. P. *Methods Enzymol.* **2001**, *339*, 204−238.
(10) Carr, H. Y.; Purcell, E. M. *Phys. Rev.* **1954**, *4*, 630−638.
(11) Meiboom, S.; Gill, D. *Rev. Sci. Instrum.* **1958**, *29*, 688−691.
(12) Korzhnev, D. M.; Salvatella, X.; Vendruscolo, M.; Di Nardo, A. A.; Davidson, A. R.; Dobson, C. M.; Kay, L. E. *Nature* **2004**, *430*, 586−590.
(13) Korzhnev, D. M.; Neudecker, P.; Zarrine-Afsar, A.; Davidson, A. R.; Kay, L. E. *Biochemistry* **2006**, *45*, 10175−10183.
(14) Korzhnev, D. M.; Bezsonova, I.; Evanics, F.; Taulier, N.; Zhou, Z.; Bai, Y.; Chalikian, T. V.; Prosser, R. S.; Kay, L. E. *J. Am. Chem. Soc.* **2006**, *128*, 5262−5269.
(15) Bezsonova, I.; Korzhnev, D. M.; Prosser, R. S.; Forman-Kay, J. D.; Kay, L. E. *Biochemistry* **2006**, *45*, 4711−4719.

populated, invisible states directly from analysis of dispersion data sets.[9] Presently such shifts, most notably ^{15}N, have been used in a very qualitative manner to infer aspects of structure.[12,16,17] However, it is clear that recording chemical shifts from additional sites would provide highly complementary and more quantitative information. For example, while ^{15}N and ^{1}HN shifts are sensitive to side-chain conformation, secondary structure, and hydrogen bonding, $^{13}C^{\alpha}$ and ^{13}CO shifts provide very powerful and more focused probes of backbone structure.[18] In addition, $^{13}C^{\alpha}$ and ^{13}CO dispersion profiles of proline residues can be measured in a facile manner, unlike the case when ^{15}N probes are used. With this in mind new dispersion[19−22] and labeling methodologies[23,24] have been developed that facilitate the measurement of shifts at many sites in "invisible" protein states beyond the backbone amide nitrogen that will significantly improve the possibilities for structural analyses. Although the relation between chemical shifts and structure remains largely empirical there have been very significant recent advances in the use of such shifts in combination with conventional molecular mechanics force fields to calculate structures of proteins.[25] The success of these methods, along with the promise for improvements in the future, has prompted us to examine closely the accuracy of backbone chemical shifts of invisible states that are derived from experimental relaxation dispersion profiles in the hopes that such shifts will be of sufficient accuracy to prove useful in structure calculations of the sort recently reported.[25]

Clearly the accuracy of chemical shifts extracted from relaxation dispersion curves depends on a large number of factors[26] including the populations and rates describing the exchange process, the exact nature of the exchange[27] (two site or more complex) and indeed also on the chemical shift differences between the states themselves. It is impossible to survey the complete array of possibilities here. Rather we record and analyze backbone ^{15}N, ^{1}HN, $^{13}C^{\alpha}$, and ^{13}CO relaxation dispersion profiles from a single exchanging system and show that accurate measures of shift differences can be obtained, at least in this case. As a guide we also carry out simulations, following Loria and co-workers,[26] that provide insight into the accuracy of the shifts that can be expected as a function of different exchanging conditions. Central to the measurement of the ^{13}C dispersion data has been the development of new labeling schemes that generate protein samples with either $^{13}C^{\alpha}$ or ^{13}CO labels that are devoid of one-bond $^{13}C-^{13}C$ homonuclear couplings[23] and the design of robust pulse schemes that exploit the labeling profiles. Here we report an experiment for measuring $^{13}C^{\alpha}$ relaxation dispersion profiles that makes use of new labeling methods as well as a pulse scheme for quantifying ^{13}CO relaxation dispersion rates that builds upon earlier work of Ishima et al.[21] The simulations and experimental data presented make it clear that for many systems accurate excited-state chemical shifts can be measured, opening the possibility for quantitative structural analyses of low populated, yet biologically important conformations.

Materials and Methods

Protein Production. The Abp1p SH3 domain[28−30] (58 residues) and a 17-residue fragment (KKTKPTPPPKPSHLKPK) from the yeast protein Ark1p peptide[31] were expressed separately in *E. coli*. BL21-(DE3) cells, as described previously.[13] The Abp1p SH3 domain was isotopically enriched by growing cells in M9 minimal media supplemented with $^{15}NH_4Cl$ as the sole nitrogen source and the appropriate carbon source, depending on the sample. Production of a ^{2}H, ^{15}N, ^{13}CO enriched sample was achieved using 2.5 g/L [1-^{13}C]-pyruvate and 5 mM (≈0.5 g/L) $NaH^{13}CO_3$ as the carbon sources, and the growth was performed in 99.9% $^{2}H_2O$ (manuscript in preparation). The culture was grown to OD ≈ 0.8 and then induced with 1 mM IPTG. At this point another 5 mM $NaH^{13}CO_3$ was added. Following an analysis of the incorporation of ^{13}C label that has been described previously,[23] it can be shown that use of the ^{13}C substrates described above produces proteins that are ^{13}CO labeled in all amino acids, with the exception of Leu and His that are not labeled at this position. Moreover, as will be described elsewhere the $^{13}C^{\alpha}$ position is labeled to less than 2%, so that complications from $^{13}CO-^{13}C^{\alpha}$ scalar couplings are minimal. It is the case, however, that other $^{13}CO-^{13}C$ scalar couplings can potentially degrade the quality of the dispersions. Ishima and Torchia[21] have considered the effects of $^{13}CO-^{13}C$ couplings in a rigorous set of simulations and shown that for scalar couplings less than 2.5 Hz and constant-time relaxation delays of 32 ms the errors introduced into measured relaxation rates are typically less than 0.5 s^{-1}. In our experience this level of error is tolerable. However, trans $^{13}CO-^{13}C$ 3-bond scalar couplings can be as large as 5 Hz,[32] and such significant couplings can degrade the quality of dispersions; dispersion profiles from the ^{13}CO groups of Trp 3 and Ala 4 showed significant artifacts (increases in transverse relaxation rates as a function of increasing numbers of refocusing pulses) and were eliminated from further analyses. In general accurate values of $^{13}CO-^{13}CO$ scalar couplings can be measured prior to an analysis of the dispersion data,[32,33] and profiles derived from residues for which couplings are ≥3−4 Hz can be eliminated.

A second sample that is ^{15}N, $^{13}C^{\alpha}$ labeled (fully protonated) was prepared in the same manner with the exception that [2-^{13}C]-glucose was used as the sole carbon source[23] and protein was expressed in H_2O media. As described previously,[23] this approach generates isolated $^{13}C^{\alpha}$ labeling at all residues with the exception of Ile, Leu, and Val (data from these three residues were not included in analyses). The small $^{13}C^{\alpha}-^{13}C^{\alpha}$ scalar couplings that are present in samples labeled in this manner (≤2 Hz[34]) will not lead to significant artifacts in dispersion profiles (see above), especially for the short constant-time relaxation elements that must be used for $^{13}C^{\alpha}$ (20 ms in the present experiments).

Samples were prepared in 50 mM sodium phosphate, 100 mM NaCl, 1 mM EDTA, and 1 mM NaN_3 pH 7.0 buffer with protein concentra-

(16) Boehr, D. D.; McElheny, D.; Dyson, H. J.; Wright, P. E. *Science* **2006**, *313*, 1638−1642.
(17) Grey, M. J.; Wang, C. Y.; Palmer, A. G. *J. Am. Chem. Soc.* **2003**, *125*, 14324−14335.
(18) Cornilescu, G.; Delaglio, F.; Bax, A. *J. Biomol. NMR* **1999**, *13*, 289−302.
(19) Korzhnev, D. M.; Neudecker, P.; Mittermaier, A.; Orekhov, V. Y.; Kay, L. E. *J. Am. Chem. Soc.* **2005**, *127*, 15602−15611.
(20) Lundstrom, P.; Vallurupalli, P.; Religa, T. L.; Dahlquist, F. W.; Kay, L. E. *J. Biomol. NMR* **2007**, *38*, 79−88.
(21) Ishima, R.; Baber, J.; Louis, J. M.; Torchia, D. A. *J. Biomol. NMR* **2004**, *29*, 187−198.
(22) Ishima, R.; Torchia, D. *J. Biomol. NMR* **2003**, *25*, 243−248.
(23) Lundstrom, P.; Teilum, K.; Carstensen, T.; Bezsonova, I.; Wiesner, S.; Hansen, D. F.; Religa, T. L.; Akke, M.; Kay, L. E. *J. Biomol. NMR* **2007**, *38*, 199−212.
(24) Teilum, K.; Brath, U.; Lundstrom, P.; Akke, M. *J. Am. Chem. Soc.* **2006**, *128*, 2506−2507.
(25) Cavalli, A.; Salvatella, X.; Dobson, C. M.; Vendruscolo, M. *Proc. Natl. Acad. Sci. U.S.A.* **2007**, *104*, 9615−9620.
(26) Kovrigin, E. L.; Kempf, J. G.; Grey, M. J.; Loria, J. P. *J. Magn. Reson.* **2006**, *180*, 93−104.
(27) Neudecker, P.; Korzhnev, D. M.; Kay, L. E. *J. Biomol. NMR* **2006**, *34*, 129−135.
(28) Rath, A.; Davidson, A. R. *Protein Sci.* **2000**, *9*, 2457−2469.
(29) Lila, T.; Drubin, D. G. *Mol. Biol. Cell* **1997**, *8*, 367−385.
(30) Drubin, D. G.; Mulholland, J.; Zhu, Z. M.; Botstein, D. *Nature* **1990**, *343*, 288−290.
(31) Haynes, J.; Garcia, B.; Stollar, E. J.; Rath, A.; Andrews, B. J.; Davidson, A. R. *Genetics* **2007**, *176*, 193−208.
(32) Hu, J. S.; Bax, A. *J. Am. Chem. Soc.* **1996**, *118*, 8170−8171.
(33) Grzesiek, S.; Bax, A. *J. Biomol. NMR* **1997**, *9*, 207−211.
(34) Peti, W.; Hennig, M.; Smith, L. J.; Schwalbe, H. *J. Am. Chem. Soc.* **2000**, *122*, 12017−12018.

tions of ≈1.4 mM. Ark1p peptide was subsequently added so that the mole fraction of the bound SH3 state was 15 and 7% for the $^{13}C^{\alpha}$- and ^{13}CO-labeled samples, respectively. Mole fractions were initially estimated from the K_D of the SH3 domain-peptide interaction ($K_D = 0.55 \pm 0.05$ μM) that was obtained from isothermal calorimetry and the known peptide/protein concentrations that were based on absorbance measurements. The fraction-bound peptide was subsequently quantified more rigorously from relaxation dispersion measurements (see Results and Discussion).

Data Acquisition and Analysis. All relaxation dispersion profiles were recorded at 25 °C using Varian Inova NMR spectrometers operating at 500 and 800 MHz (^1H frequency), equipped with room-temperature triple resonance probeheads. Constant-time,[35] relaxation compensated[36] pulse schemes have been employed for all measurements. ^{15}N dispersion profiles were generated using a TROSY-based pulse scheme[37] (identical exchange parameters were obtained using sequences that did not involve exchange of TROSY magnetization[38,39]). ^1H relaxation rates were measured using the scheme of Ishima et al.,[22] while $^{13}C^{\alpha}$ and ^{13}CO data sets were obtained using pulse sequences that are presented herein.

^{15}N, ^{13}CO, and ^1HN relaxation dispersion profiles were recorded on the ^{13}CO labeled SH3-peptide complex. Eighteen values of ν_{CPMG} (see below) ranging from 33 to 1000 Hz were obtained for the ^{15}N (total acquisition times of 12 and 15 h at 500 and 800 MHz, respectively) and ^{13}CO relaxation measurements (acquisition times of 25 and 15 h at 500 and 800 MHz), while 18 values between 66 and 2000 Hz were employed in the ^1HN experiments (20 h net acquisition times at both 500 and 800 MHz). A constant-time relaxation delay of 30 ms was used in all experiments. ^{15}N and $^{13}C^{\alpha}$ relaxation dispersion experiments were performed on the $^{13}C^{\alpha}$ labeled SH3-peptide complex with between 17 and 19 ν_{CPMG} values ranging from 50 to 1000 Hz obtained in each set of experiments. Experiment durations were 13 (500 MHz) and 16 h (800 MHz) for recording the ^{15}N profiles and 51 (500 MHz) and 39 h (800 MHz) for the $^{13}C^{\alpha}$ measurements. A constant relaxation time of 20 ms was used throughout. Scalar evolution due to $^{15}N-^{13}CO$ or $^{15}N-^{13}C^{\alpha}$ couplings during constant-time CPMG relaxation delays was not corrected for in the analysis of the dispersion data. However, as discussed by Ishima and Torchia[21] these effects are expected to be negligible (well under 1% error) for the ν_{CPMG} values used in the present set of experiments.

Dispersion data sets for the different spin probes were recorded sequentially, although for a given nucleus type different ν_{CPMG} values were interleaved. The extent of sample heating in each of the dispersion experiments was evaluated by monitoring the movement of peak positions in 1D spectra recorded immediately after steady state was achieved. Heating effects are very small for the ^{15}N, ^{13}CO, and ^1HN measurements, but can be as much as 1.4 °C in $^{13}C^{\alpha}$ dispersion experiments. In the latter case this was compensated for by a decrease in the setting of the variable temperature unit.

Of the four types of data sets recorded (corresponding to dispersions from ^{15}N, ^1HN, $^{13}C^{\alpha}$, and ^{13}CO) it is clear that the ^{15}N profiles are of the highest sensitivity and that the ^{13}C-based experiments are of the lowest. On average a factor of 2.3 separates the signal-to-noise values in ^{15}N and $^{13}C^{\alpha}$ dispersion data sets recorded for this study (spectra with $\nu_{CPMG} = 1000$ Hz compared in both cases). In large part the decrease in sensitivity results from the carbon labeling schemes that have been used,[23] (see above) but in the case of $^{13}C^{\alpha}$ there is an additional contribution to the decreased sensitivity. This derives from the $^1H^{\alpha}-^{13}C^{\alpha}$ dipolar interaction, 2-fold larger than for $^1HN-^{15}N$, leading to a 4-fold increase in the dipolar-derived transverse relaxation rate for $^{13}C^{\alpha}$. In principle, a factor of 2 increase in sensitivity in all data sets could be obtained by recording spectra on spectrometers equipped with cryogenically cooled probe-heads (all of the data were recorded on room-temperature probes) that would be particularly beneficial for the ^{13}C data, although we have not done so here.

Data sets were processed and analyzed with the NMRPipe program[40] and signal intensities quantified using the program FuDA (smk@kiku.dk). Relaxation dispersion profiles, $R_{2,eff}(\nu_{CPMG})$, were generated from peak intensities, $I_1(\nu_{CPMG})$, in a series of 2D $^1HN-^{15}N$ (^{15}N, ^{13}CO, and ^1HN CPMG experiments) or $^1H^{\alpha}-^{13}C^{\alpha}$ ($^{13}C^{\alpha}$ experiments) correlation maps measured as a function of CPMG frequency,[35] $\nu_{CPMG} = 1/(4\tau_{CP})$, where $2\tau_{CP}$ is the interval between consecutive refocusing pulses of the CPMG sequence. Peak intensities were converted into effective relaxation rates via $R_{2,eff}(\nu_{CPMG}) = -1/T_{relax} \ln(I_1(\nu_{CPMG})/I_0)$, where I_0 is the peak intensity in a reference spectrum recorded without the relaxation delay T_{relax}.

Values of the exchange rate, k_{ex}, the population of the invisible state, p_B, chemical shift differences between states, $\Delta\tilde{\omega}$, and intrinsic relaxation rates were extracted using in-house written software by minimization of the following χ^2 target function:

$$\chi^2(\zeta) = \sum \frac{(R_{2,eff}^{clc}(\zeta) - R_{2,eff}^{exp})^2}{(\Delta R_{2,eff}^{exp})^2} \quad (1)$$

where $R_{2,eff}^{exp}$ and $\Delta R_{2,eff}^{exp}$ are experimental effective relaxation rates and their uncertainties, respectively, $R_{2,eff}^{clc}(\zeta)$ are model relaxation rates obtained by numerical integration of the Bloch−McConnell equations[41] for a two-site chemical exchange model, ζ denotes the set of adjustable model parameters, and the summation in eq 1 is over the number of experimental data points. In all fits of experimental dispersion profiles we have assumed that the intrinsic relaxation rates were the same for both exchanging states. Palmer and co-workers have defined the exchange limits for which this is a valid assumption[42] and for the systems considered here this approximation is justified. Indeed, we showed previously through a series of simulations that even if the exchange is between folded and unfolded protein states where the intrinsic relaxation rates are significantly different the assumption of equal rates does not introduce appreciable errors into the extracted exchange parameters.[43]

Dispersion profiles from separate residues recorded at 500 and 800 MHz were analyzed together to extract exchange parameters and shift differences (data sets from a given nucleus type, ^{15}N, ^1HN, $^{13}C^{\alpha}$, or ^{13}CO, were analyzed independently to establish that similar exchange rates and populations are extracted with the different probes). After fitting all dispersion profiles, residues were excluded if (i) the two-site model did not generate statistically significant improvements in fits over a model of no exchange at the 98% confidence level or (ii) if the reduced χ^2 value for fits of an individual profile was greater than 1.5. Using these criteria, profiles from 43, 29, and 33 residues were retained from the preliminary analysis of ^{15}N, ^{13}CO, and ^1HN dispersion profiles, respectively (measured on the ^{13}CO labeled sample). In a similar manner, profiles from 36 (^{15}N) and 27 ($^{13}C^{\alpha}$) residues were retained from data sets recorded on the $^{13}C^{\alpha}$ labeled sample.

Signs of chemical shift differences for ^{15}N, ^{13}CO, and $^{13}C^{\alpha}$ nuclei were obtained by the method of Skrynnikov et al.[44] Briefly, to obtain the signs of ^{15}N chemical shifts $^1HN-^{15}N$ HSQC and HMQC data sets were recorded at 500 and 800 MHz and the position of correlations

(35) Mulder, F. A. A.; Skrynnikov, N. R.; Hon, B.; Dahlquist, F. W.; Kay, L. E. *J. Am. Chem. Soc.* **2001**, *123*, 967−975.
(36) Loria, J. P.; Rance, M.; Palmer, A. G. *J. Am. Chem. Soc.* **1999**, *121*, 2331−2332.
(37) Loria, J. P.; Rance, M.; Palmer, A. G. *J. Biomol. NMR* **1999**, *15*, 151−155.
(38) Tollinger, M.; Skrynnikov, N. R.; Mulder, F. A. A.; Forman-Kay, J. D.; Kay, L. E. *J. Am. Chem. Soc.* **2001**, *123*, 11341−11352.
(39) Hansen, D. F.; Vallurupalli, P.; Kay, L. E. *J. Phys. Chem. B*, published online Nov. 15, 2007. PMID: 18001083
(40) Delaglio, F.; Grzesiek, S.; Vuister, G. W.; Zhu, G.; Pfeifer, J.; Bax, A. *J. Biomol. NMR* **1995**, *6*, 277−293.
(41) McConnell, H. M. *J. Chem. Phys.* **1958**, *28*, 430−431.
(42) Millet, O.; Loria, J. P.; Kroenke, C. D.; Pons, M.; Palmer, A. G. *J. Am. Chem. Soc.* **2000**, *122*, 2867−2877.
(43) Orekhov, V. Y.; Korzhnev, D. M.; Kay, L. E. *J. Am. Chem. Soc.* **2004**, *126*, 1886−1891.
(44) Skrynnikov, N. R.; Dahlquist, F. W.; Kay, L. E. *J. Am. Chem. Soc.* **2002**, *124*, 12352−12360.

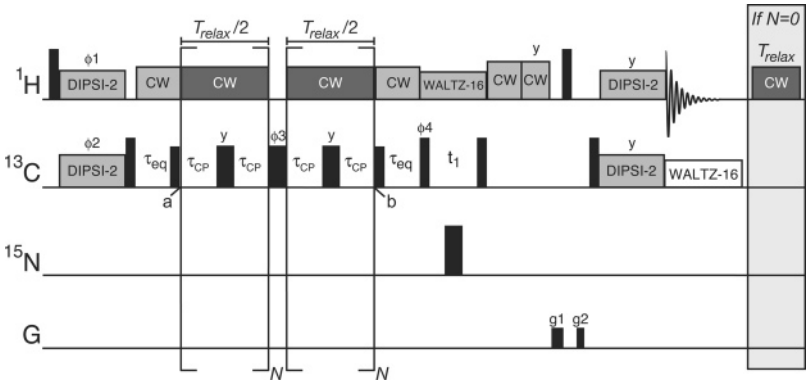

Figure 1. Pulse scheme of the $^{13}C^{\alpha}$ constant-time relaxation dispersion experiment for measuring millisecond time-scale dynamics in proteins. All ^{1}H and ^{13}C 90° (180°) radio frequency (rf) pulses are shown as narrow (wide) black bars and are applied at the highest possible power level, with the exception of the ^{13}C refocusing pulses of the CPMG element between points *a* and *b*, along with the 90° sandwiching pulses, which are applied at a slightly lower power level (≈16 kHz). All pulse phases are assumed to be *x*, unless indicated otherwise. In principle, the ^{13}C refocusing pulses between points *a* and *b* could be applied with the RE-BURP profile[57] so that three-bond $^{13}C^{\alpha}-^{13}CO$ couplings in GLX residues are refocused (not done here). The ^{1}H carrier is placed on the water signal (4.77 ppm), while the ^{13}C rf carrier is at 55 ppm. Transfer of magnetization from ^{1}H to ^{13}C and back is achieved using $^1H-^{13}C$ heteronuclear cross polarization with DIPSI-2 mixing schemes[58,59] (duration of 7.6 ms) with matched ^{1}H and ^{13}C fields of approximately 8 kHz. Delays of $\tau_{eq} = 5$ ms equilibrate magnetization prior to and after the CPMG relaxation interval. Proton continuous wave (CW) decoupling during the CPMG period eliminates evolution due to the one-bond $^1H^{\alpha}-^{13}C^{\alpha}$ scalar coupling and is applied at a field strength of approximately 14 kHz; the exact field strength varies slightly (≈10%) for different values of *N*, as described previously[39] and in the text. Other elements labeled CW ensure dephasing of water magnetization. The CW elements immediately after the t_1 period are of durations 4 and 2.5 ms, respectively, and are applied at a field strength of 16 kHz. A CW element is applied for a duration of T_{relax} immediately after acquisition in the case where $N = 0$ to keep heating constant for all values *N*. ^{1}H decoupling during t_1 was achieved with a WALTZ-16 scheme[60] applied at a field of 5 kHz while ^{13}C decoupling during acquisition employed a 2.2 kHz field. The phase cycling used is $\phi 1 = 2\{y\}, 2\{-y\}$; $\phi 2 = 2\{y\}, 4\{-y\}, 2\{y\}$; $\phi 3 = 8\{x\}, 8\{-x\}$; $\phi 4 = \{x, -x\}$; receiver $= 2\{x, -x\}, 2\{-x, x\}$. The value of T_{relax} is chosen such that approximately 50% of the signal is reduced relative to $T_{relax} = 0$, as described previously.[35] Quadrature detection in the indirect dimension is obtained via State-TPPI[61] of $\phi 4$. Gradient strengths G/cm (length in ms) are $g1 = 24.0(3)$, $g2 = 26.5(1)$.

compared in (i) HMQC and HSQC maps obtained at 500 MHz, (ii) HMQC and HSQC maps obtained at 800 MHz, and (iii) HSQC maps generated at 500 and 800 MHz. In the few cases where conflicting results were obtained via i−iii, the sign was based on the comparison that showed the largest difference in peak positions. In a similar manner $^1HN-^{13}CO$ planes from HNCO data sets[45] were recorded at 500 and 800 MHz to obtain the signs of the ^{13}CO chemical shifts, with the ^{13}CO chemical shift recorded either from evolution of single-quantum or multiple-quantum (^{15}N-^{13}CO) coherences. Finally, the signs of the $^{13}C^{\alpha}$ chemical shifts were determined from a comparison of ($^{13}C^{\alpha,1}H^{\alpha}$) data sets recorded at 500 and 800 MHz using the scheme of Figure 1 with $T_{relax} = 0$.

Simulations. ^{15}N relaxation dispersion profiles were computed at both 500 and 800 MHz assuming a two-site exchange model by solving the Bloch−McConnell equations[41] with values of ν_{CPMG} identical to those used experimentally. Chemical shift differences, identical to those obtained from fits of experimental ^{15}N data sets (36 residues, $^{13}C^{\alpha}$-sample), and experimentally derived intrinsic relaxation rates, were used as input. Thus a total of 36 pairs of dispersion curves (1 each for 500 and 800 MHz) were calculated. Computations were performed for 10 values of p_B, equally spaced between 0 and 20% and 16 values of k_{ex} such that $100\ s^{-1} \le k_{ex} \le 3000\ s^{-1}$. Residues were removed from analysis if $R_{2,eff} > 75\ s^{-1}$ for one or more ν_{CPMG} value in the dispersion profile calculated at either 500 or 800 MHz (such large values of $R_{2,eff}$ would give rise to very weak peaks in correlation spectra). Gaussian errors corresponding to 5% of $R_{2,eff}$ or $0.5\ s^{-1}$ (whichever is largest) were introduced into each profile.[26] For each (p_B,k_{ex}) value all of the computed data sets were subsequently fit simultaneously, exactly as for the experimental data, and the values of $|\Delta\varpi_{CPMG}|$ obtained from fits of the simulated data used to produce correlations of $|\Delta\varpi_{CPMG}|$ versus $|\Delta\varpi_{INPUT}|$ that were then fit to an equation of the form $y = mx$. A total of 60 data sets were analyzed in this way for each (p_B,k_{ex}), corresponding to profiles with different Gaussian errors, and the average value of *m* and its standard deviation calculated and analyzed as described in the text. The process was repeated for each of the 160 (p_B,k_{ex}) combinations.

Results and Discussion

Experimental Approach. A major objective of the present study is to evaluate the accuracy of experimentally extracted backbone chemical shift values of low populated, invisible states by relaxation dispersion NMR spectroscopy as a prelude to using such shifts as probes of molecular structure. Our interest is in systems for which a substantial number of residues report on the exchange event, enabling the extraction of large numbers of chemical shifts. Examples include enzymes undergoing conformational changes during catalysis,[16,46−48] proteins undergoing folding/unfolding transitions,[12,49,50] and receptors that must change conformation on a millisecond time-scale to accommodate the binding of ligands.[51] A difficulty emerges in establishing the accuracy of the extracted experimental chemical shifts via relaxation dispersion since for most systems they cannot be obtained in any other way for comparison. Some information about the accuracy of the measurements can be obtained from studies of protein folding where ^{15}N chemical shifts of the invisible unfolded state have been extracted.[12,52] Typically, pairwise rmsd values between these shifts and the corresponding random coil values that have been tabulated on the basis of studies of peptides[53,54] are on the order of 1 ppm.[52] Are the differences a reflection of experimental errors in measured dispersion values or do they reflect potentially the nonrandom coil nature of the unfolded state? Although it is clear

(45) Kay, L. E.; Ikura, M.; Tschudin, R.; Bax, A. *J. Magn. Reson.* **1990**, *89*, 496−514.
(46) Eisenmesser, E. Z.; Bosco, D. A.; Akke, M.; Kern, D. *Science* **2002**, *295*, 1520−1523.
(47) Eisenmesser, E. Z.; Millet, O.; Labeikovsky, W.; Korzhnev, D. M.; Wolf-Watz, M.; Bosco, D. A.; Skalicky, J. J.; Kay, L. E.; Kern, D. *Nature* **2005**, *438*, 117−121.
(48) Wolf-Watz, M.; Thai, V.; Henzler-Wildman, K.; Hadjipavlou, G.; Eisenmesser, E. Z.; Kern, D. *Nat. Struct. Mol. Biol.* **2004**, *11*, 945−949.
(49) Sugase, K.; Dyson, H. J.; Wright, P. E. *Nature* **2007**, *447*, 1021−1024.
(50) Zeeb, M.; Balbach, J. *J. Am. Chem. Soc.* **2005**, *127*, 13207−13212.
(51) Mulder, F. A. A.; Mittermaier, A.; Hon, B.; Dahlquist, F. W.; Kay, L. E. *Nat. Struct. Biol.* **2001**, *8*, 932−935.
(52) Neudecker, P.; Zarrine-Afsar, A.; Choy, W. Y.; Muhandiram, D. R.; Davidson, A. R.; Kay, L. E. *J. Mol. Biol.* **2006**, *363*, 958−976.
(53) Schwarzinger, S.; Kroon, G. J.; Foss, T. R.; Chung, J.; Wright, P. E.; Dyson, H. J. *J. Am. Chem. Soc.* **2001**, *123*, 2970−2978.
(54) Wishart, D. S.; Bigam, C. G.; Holm, A.; Hodges, R. S.; Sykes, B. D. *J. Biomol. NMR* **1995**, *5*, 67−81.

from these results that an upper bound on the accuracy of extracted shifts is ca. 1 ppm it is difficult to establish what the lower bound might be, and this has important implications in addressing the utility of relaxation dispersion-based chemical shifts in structural studies.

To quantify the accuracy of extracted shifts still further a system must be chosen where the chemical shifts of the excited-state are known from some other method. Here we use a protein/ligand exchanging system that is well described by the two-site exchange model (see later)

$$\mathrm{P} + \mathrm{L} \underset{k_{\mathrm{off}}}{\overset{k_{\mathrm{on}}}{\rightleftharpoons}} \mathrm{PL} \qquad (2)$$

where P and L correspond to protein and ligand that bind on a time-scale that is within the window of the dispersion experiment. The accuracy of shift differences (in ppm), $\Delta\varpi$, extracted from dispersion profiles generated on such a system can be ascertained in a straightforward manner by comparing $\Delta\varpi$ with corresponding values obtained from chemical shifts measured directly on apo and fully bound samples. In the application considered below P is the WT SH3 domain from the yeast cytoskeleton protein Abp1p (ref 28−30) and L is a 17 residue target peptide[31] from the protein Ark1p. Unlike the G48M mutant of the Abp1p SH3 domain or the corresponding mutant of the Fyn SH3 domain in which the apo-forms of the protein produce large dispersion profiles due to a protein folding transition that we have monitored previously,[13] the WT Abp1p SH3 domain does not show dispersions in the absence of added peptide. Here a pair of studies were performed on fractionally bound protein where $p_B = [PL]/([P] + [PL])$ was either 7% (^{13}CO labeled sample) or 15% ($^{13}C^{\alpha}$ labeled sample), so that only peaks corresponding to the P state were observed in spectra, with dispersion curves reporting on the chemical shift differences between bound and free states of the SH3 domain. The distinct p_B values for the two samples allow an evaluation of the accuracy of the derived chemical shifts for a pair of different exchanging conditions.

Experimental Methodology. As described in the Materials and Methods section ^{15}N and ^{1}HN dispersion profiles were obtained using constant-time,[35] relaxation-compensated[36] pulse schemes that are described in the literature,[22,37] while ^{13}CO dispersions were recoded using a modified version of the experiment published by Ishima et al.[21] (Supporting Information, Figure 1). $^{13}C^{\alpha}$ chemical shifts are a particularly valuable probe of protein secondary structure,[55,56] and they have been measured for the invisible bound state of the Abp1p SH3 domain using a pulse scheme that records $^{13}C^{\alpha}$-dispersions for proteins labeled according to the protocol described in Materials and Methods (that does not produce $^{13}C^{\alpha}-^{13}C^{\beta}$ or $^{13}C^{\alpha}-^{13}$CO spin pairs), Figure 1.

The pulse scheme that has been developed follows directly from an improved ^{15}N-based CPMG dispersion experiment that we have recently published.[39] Central to the experiment is a constant-time CPMG relaxation interval between points *a* and *b* during which a variable number of ^{13}C 180° refocusing pulses are applied. A series of 2D ($^{13}C^{\alpha}$,$^{1}H^{\alpha}$) correlation maps are recorded, each corresponding to a fixed number of ^{13}C pulses, from which effective $^{13}C^{\alpha}$ relaxation rates, $R_{2,\mathrm{eff}}$, are calculated (see Materials and Methods). Because we prefer to record both ^{15}N and $^{13}C^{\alpha}$ dispersions on the same sample the protein must be dissolved in $^{1}H_2O$, requiring excellent solvent suppression since $^{1}H^{\alpha}$ shifts can potentially be very close to the water line. Here this is achieved through the almost continuous application of ^{1}H RF, including during the initial and final magnetization transfer steps that are based on ^{1}H,^{13}C heteronuclear cross-polarization schemes.[58,59] Magnetization is maintained in-phase during the constant-time CPMG relaxation interval through application of a ^{1}H CW field of strength (Hz) $\nu_{CW} = 2k\nu_{CPMG}$, where $\nu_{CPMG} = (4\tau_{CP} + 2\mathrm{pwc})^{-1}$, pwc is the 180° ^{13}C pulse-width and k is an integer;[39,62] values of ν_{CW} vary by no more than 8% for the values of ν_{CPMG} used to record dispersion profiles when a mean ν_{CW} field of ca. 13−15 kHz is used. In this manner relaxation rates during the pulse train are given by $R_{C,I}$, rather than $1/2(R_{C,I} + R_{C,A})$, as would be the case in sequences without ^{1}H decoupling, where $R_{C,I}$ and $R_{C,A}$ are decay rates of in-phase and anti-phase $^{13}C^{\alpha}$ magnetization, respectively. Since for macromolecular applications $R_{C,I} < R_{C,A}$, significant sensitivity gains can be achieved with this scheme.[39] Finally, it is noteworthy that application of the ^{13}C $180^{\circ}_{\phi 3}$ ($\phi 3 = \pm x$) pulse in the center of the CPMG interval minimizes artefacts due to refocusing imperfections during the CPMG pulse train, as described previously.[39]

Applications to the Abp1p SH3−Ark1p Peptide System. Figure 2 shows selected ^{15}N (A), ^{1}HN (B), $^{13}C^{\alpha}$ (C), and ^{13}CO (D) relaxation dispersion profiles for Ser 52 of the Abp1p SH3 domain−peptide system, obtained from measurements on samples with 7% or 15% mole fractions of peptide (see earlier). Experimental data (circles) have been recorded at static magnetic field strengths of 500 and 800 MHz (^{1}H frequency), and all dispersion profiles from a given nucleus (^{15}N, ^{1}HN, $^{13}C^{\alpha}$, and ^{13}CO) fit globally and independently to extract $k_{on}[L]$ and k_{off} as well as residue specific $|\Delta\varpi|$ values and intrinsic relaxation rates at each magnetic field. Figure 2 illustrates that the intrinsic relaxation rates do indeed differ with field, in particular for ^{1}HN and ^{13}CO. These differences are, in large part, in keeping with expectations based on chemical shift anisotropy (CSA) values that can be quite substantial, even for amide protons where values for the anisotropy are on average 10 ppm for residues in the β-sheet conformation.[63] Notably, ^{15}N dispersion profiles do not cross for Ser 52 (nor for Asn 53), although they do for the majority of residues as expected since TROSY-based versions of the ^{15}N dispersion experiment[37] are used. In the case of Ser 52 the ^{15}N CSA may be smaller than average or additional very fast exchange processes may contribute to the relaxation rates that would not be quenched by the CPMG fields used presently.

Values of p_B and $k_{ex} = k_{on}[L] + k_{off}$, obtained from independent fits of ^{15}N, ^{13}CO, and ^{1}HN dispersion data recorded on the ^{13}CO-labeled Abp1p SH3 domain sample, are (7.2%, 263 s^{-1}), (7.5%, 247 s^{-1}), and (7.2%, 236 s^{-1}), respectively. Distributions of exchange parameters that are consistent with the experimental data have been obtained from a bootstrap

(55) Spera, S.; Bax, A. *J. Am. Chem. Soc.* **1991**, *113*, 5490−5492.
(56) Wishart, D. S.; Sykes, B. D. *J. Biomol. NMR* **1994**, *4*, 171−180.
(57) Geen, H.; Freeman, R. *J. Magn. Reson.* **1991**, *93*, 93−141.
(58) Zuiderweg, E. R. *J. Magn. Reson.* **1990**, *89*, 533−542.
(59) Brown, L. R.; Sanctuary, B. C. *J. Magn. Reson.* **1991**, *91*, 413−421.
(60) Shaka, A. J.; Keeler, J.; Frenkiel, T.; Freeman, R. *J. Magn. Reson.* **1983**, *52*, 335−338.
(61) Marion, D.; Ikura, M.; Tschudin, R.; Bax, A. *J. Magn. Reson.* **1989**, *85*, 393−399.
(62) Vallurupalli, P.; Scott, L.; Williamson, J. R.; Kay, L. E. *J. Biomol. NMR* **2007**, *38*, 41−46.
(63) Cornilescu, G.; Bax, A. *J. Am. Chem. Soc.* **2000**, *122*, 10143−10154.

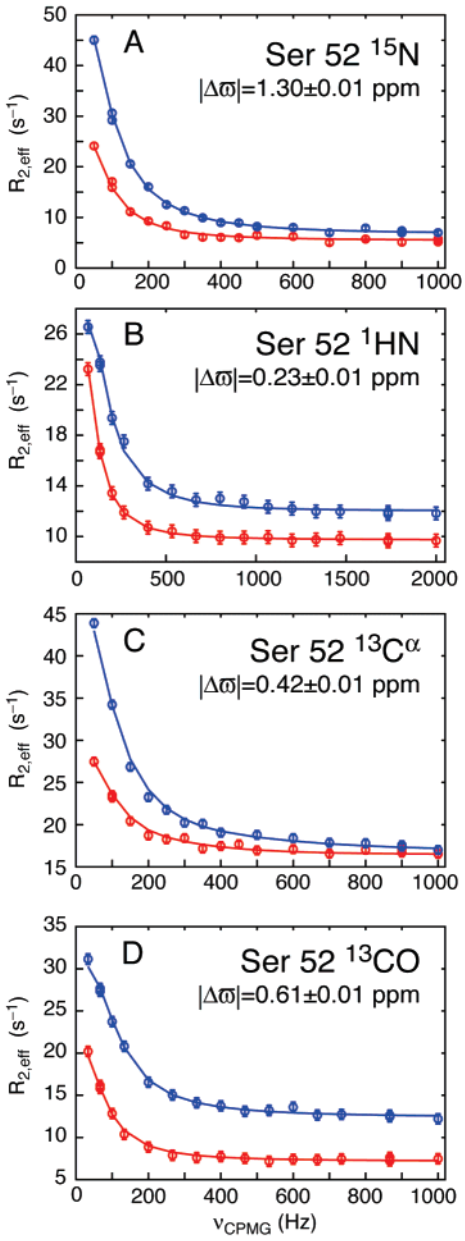

Figure 2. ^{15}N, ^{1}HN, ^{13}Cα, and ^{13}CO relaxation dispersion profiles (circles) for Ser 52, along with $|\Delta\varpi|$ extracted from fits (solid lines). Data sets are recorded at 800 MHz (blue) and 500 MHz (red), 25 °C. The ^{15}N dispersion profiles were recorded using an experiment in which the exchange of TROSY magnetization components is measured.[37] The ^{15}N, ^{1}HN, and ^{13}CO (^{13}Cα) profiles were obtained from measurements recorded on the ^{13}CO (^{13}Cα) labeled SH3 domain−peptide complex containing 7% (15%) mole-fraction-bound peptide.

procedure[64] where data sets from ^{15}N, ^{1}HN, ^{13}Cα, and ^{13}CO are treated independently. Here each of the k residues for which dispersion profiles are obtained at *both* 500 and 800 MHz (see Materials and Methods for selection criteria and the values of k) for a given type of probe (for example, ^{15}N or ^{13}Cα) are numbered from 1 to k, a set of random numbers between 1 and k generated, and the pair of experimental dispersion profiles (500 and 800 MHz) of residue $j \in \{1...k\}$ selected each time j appears in the set of k random numbers. The k pairs of experimental dispersion profiles chosen in this manner are fit globally to produce values of (p_B,k_{ex}) and the procedure repeated

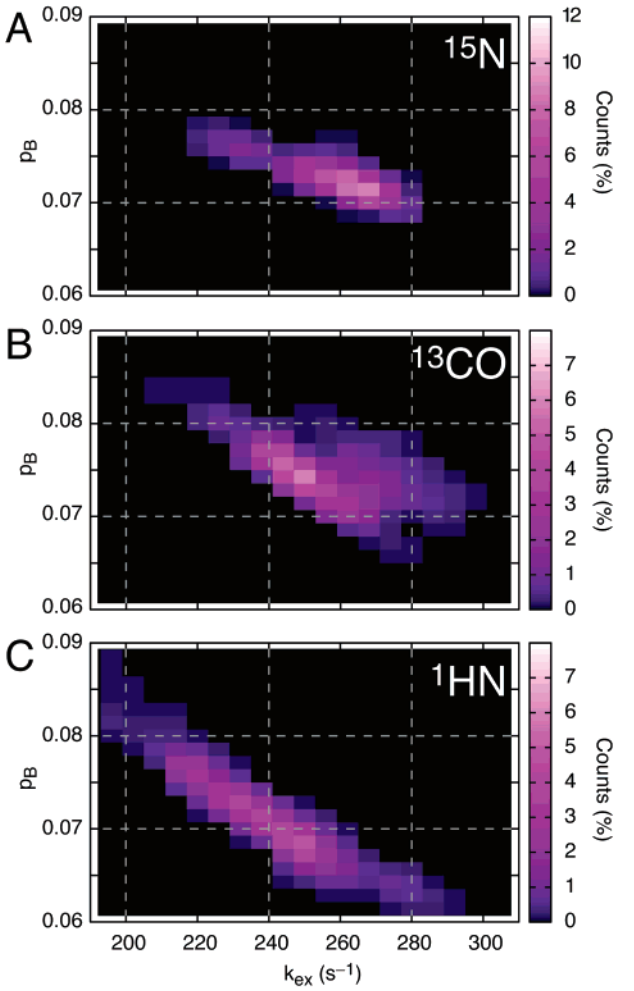

Figure 3. Distribution of (p_B,k_{ex}) values obtained from fits of ^{15}N (A), ^{13}CO (B), and ^{1}HN (C) dispersion profiles measured on the ^{13}CO-labeled sample, 25 °C. The bootstrap procedure[64] used to generate the distribution of exchange parameters that is consistent with the experimental data is described in the text.

200 times, with the results contoured as in Figure 3A−C. It is noteworthy that the range of (p_B,k_{ex}) values can be quite substantial, especially for exchange parameters obtained from fits of ^{1}HN dispersion data.

Average values of (p_B,k_{ex}) = (15.6%, 365 s^{-1}) and (15.1%, 438 s^{-1}) are obtained from fits of ^{15}N and ^{13}Cα dispersion profiles measured on the ^{13}Cα-labeled Abp1p SH3 sample, with the distribution of parameters indicated in Figure 4. Although the average values of k_{ex} obtained from fits of ^{15}N and ^{13}Cα probes differ by 20%, there is a wide distribution of k_{ex} values from the ^{13}Cα data and the distribution overlaps with that obtained from ^{15}N. Interestingly, the (p_B,k_{ex}) surface in Figure 4B is very shallow so that (i) the goodness of fit (χ^2 of eq 1) of the ^{13}Cα data is not degraded when values of exchange parameters (p_B,k_{ex}) obtained from the ^{15}N data are imposed in fits of the carbon dispersion profiles (see below) and (ii) essentially the same values of $\Delta\varpi$ are obtained in cases where (p_B,k_{ex}) = (15.6%, 365 s^{-1}) or 15.1%, 438 s^{-1}) (rmsd of 0.013 ppm, see below). The large surface for the ^{13}Cα data (Figure 4B) relative to what is observed for ^{15}N (Figure 4A) reflects, in large part, the smaller range of chemical shift differences (in Hz, see below) that are observed for carbon. Indeed, when a smaller ^{15}N data set with shift differences ≤1.75 ppm is chosen

(64) Efron, B.; Tibshirani, R. *Stat. Sci.* **1986**, *1*, 54−77.

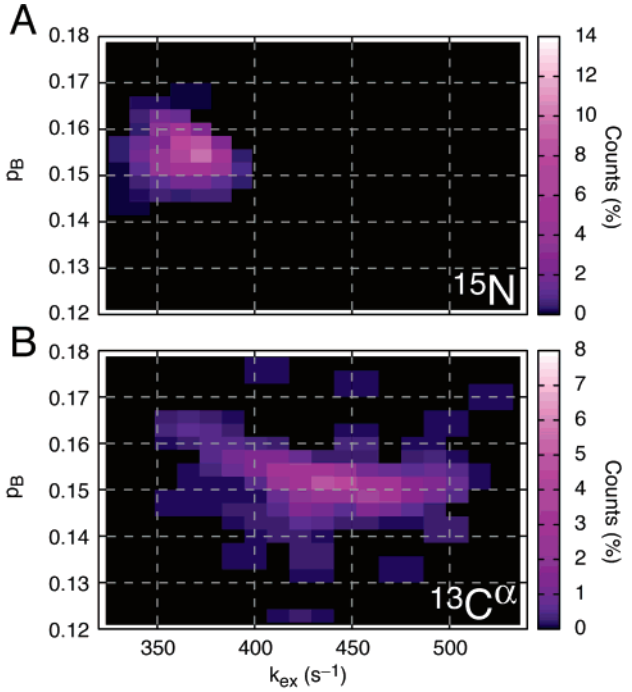

Figure 4. Distribution of (p_B,k_{ex}) values obtained from fits of ^{15}N (A) and ^{13}C$^{\alpha}$ (B) dispersion profiles measured on the ^{13}C$^{\alpha}$ -labeled sample, 25 °C.

for analysis the range of p_B values increases substantially (from 0.13 to 0.18), although the center of the distribution is very similar to what is observed in Figure 4A. It is clear that for the majority of the data sets, with the exception of perhaps ^{15}N where a large number of residues can be obtained, where the sensitivity is highest, and where the distribution of shift differences is such that often a wide range of chemical exchange regimes is sampled, there is a correlation between p_B and k_{ex}. In general, a robust approach for analysis would be to fit data from the different nuclei together to get the best measure of global exchange parameters for extraction of $\Delta\varpi$ values, although as we show below very accurate values of shift differences are obtained in fits of each probe (^{15}N, ^{1}HN, ^{13}C$^{\alpha}$, and ^{13}CO) separately.

Finally, it is of interest that k_{ex} values are somewhat different for the ^{13}C$^{\alpha}$- and ^{13}CO-labeled samples. This is as expected. The smaller k_{ex} value for the ^{13}CO sample ($\approx$245 s^{-1} vs $\approx$310 s^{-1}) arises from the smaller p_B value (i.e., less peptide was used in this case) that leads to a decrease in [L] relative to the ^{13}C$^{\alpha}$-labeled sample.

Figure 5 plots $\Delta\varpi$ values obtained from fits of ^{13}CO (A) and ^{1}HN (B) relaxation dispersion data (Y axis) vs $\Delta\varpi$ calculated from SH3 domain chemical shifts measured from samples where either P or PL is the dominant species (X axis, $\Delta\varpi_{Direct}$). Only the absolute values of the shift differences between states can be obtained directly from relaxation dispersion measurements.[9] However, it is possible to determine the sign of the difference in the shifts, and hence the chemical shifts of the excited state, by comparing the positions of correlations of the ground state in HSQC and HMQC type spectra recorded at a single field or in HSQC data sets obtained at multiple fields, as described previously.[44] Such an analysis has been performed here for residues with $|\Delta\varpi_{CPMG}| > 0.1$ ppm (Figure 5A), where the sign is explicitly included in the figure by multiplication of $|\Delta\varpi_{CPMG}|$ by "Sign", the sign of the shift difference obtained

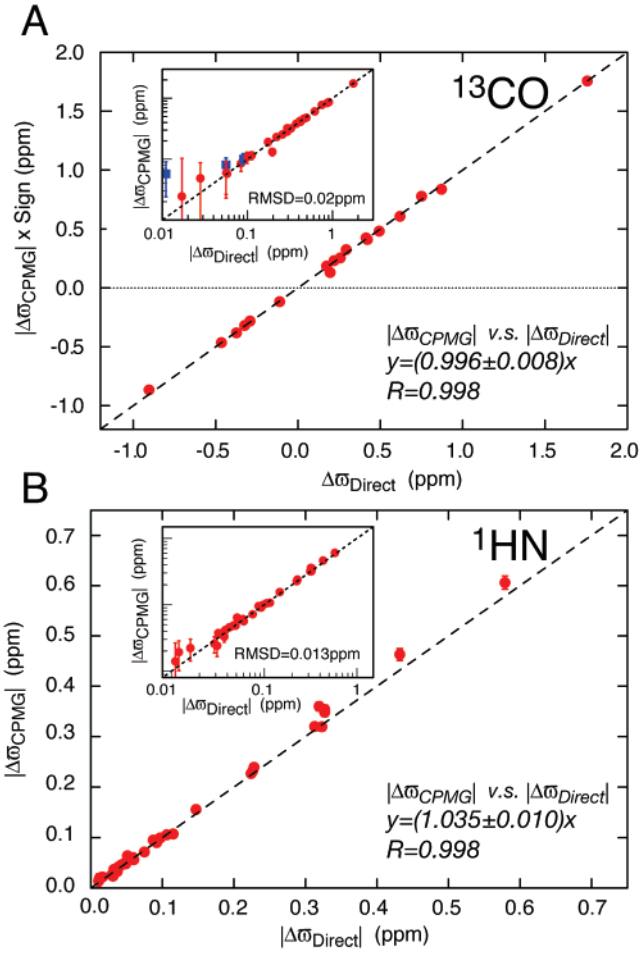

Figure 5. Correlation between $\Delta\varpi$ values (ppm) extracted from fits of relaxation dispersion data (Y axis, including signs of the shift differences in A) versus $\Delta\varpi$ values measured directly from samples of the free and fully bound SH3 domain. Points in red are those for which the sign of $\Delta\varpi$ obtained by the method of Skrynnikov et al.[44] is correct while the blue points (inset in A) refer to those for which an incorrect sign was obtained. The dashed line corresponds to $|\Delta\varpi_{CPMG}| = |\Delta\varpi_{Direct}|$; the slope of the best fit ($y = mx$) line along with the value of Pearson's correlation coefficient are shown. Only points for which $|\Delta\varpi| > 0.1$ ppm are retained in the main figures. Insets show log/log plots, with all of the extracted $|\Delta\varpi|$ values illustrated. The rmsd values between $|\Delta\varpi_{CPMG}|$ and $|\Delta\varpi_{Direct}|$ are indicated in the insets and include all chemical shift differences that were quantified (i.e., all points in the log/log plot). Chemical shifts were obtained from dispersions recorded on the ^{13}CO labeled sample.

experimentally. All of the signs of the shift differences for the 18 residues for which $|\Delta\varpi_{CPMG}| > 0.1$ ppm have been determined correctly. It is also possible to obtain the signs of the ^{1}HN shift differences by recording and analyzing ^{1}H−^{15}N double- and zero-quantum dispersion profiles, making use of the previously determined signs of the ^{15}N chemical shifts of the excited state, as has been done previously;[19,65] however, such an analysis has not been performed here. Thus, only the absolute values of $\Delta\varpi$ are plotted for ^{1}HN in Figure 5B. The accuracy of the extracted $|\Delta\varpi|$ values is very high, with slopes of linear correlation plots of 1.0 and 1.04 for the ^{13}CO and ^{1}HN $\Delta\varpi$ values, respectively, and correlation coefficients of greater than 0.99. Accurate measurements of $|\Delta\varpi|$ are obtained even for very small shift differences (as small as 0.02 ppm), as indicated in the insets to each of the plots where the correlations are

(65) Kloiber, K.; Konrat, R. *J. Biomol. NMR* **2000**, *18*, 33−42.

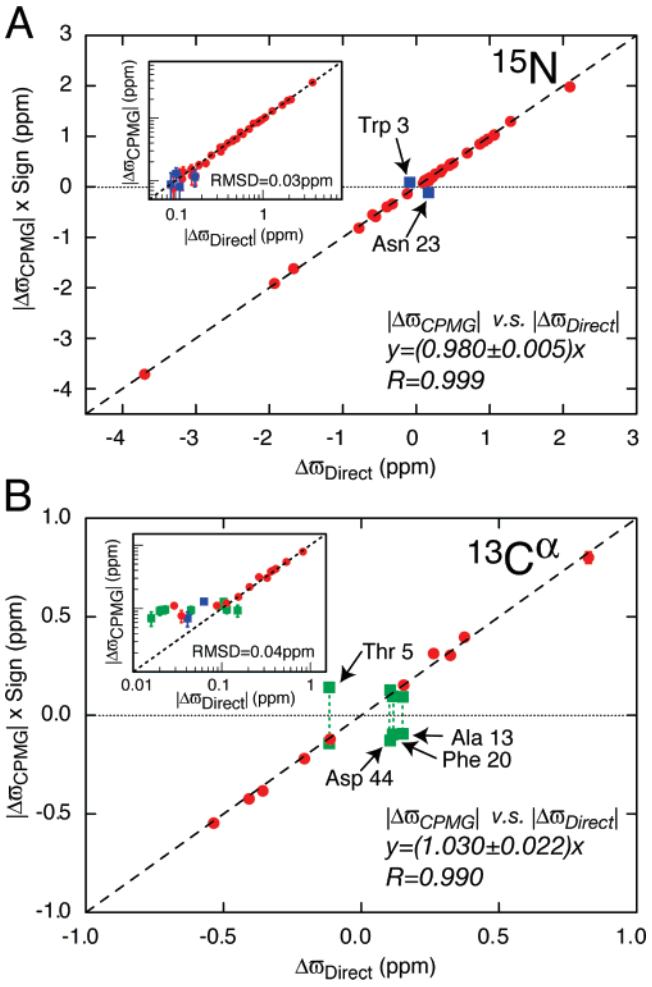

Figure 6. Correlation between $\Delta\varpi$ values (ppm) extracted from fits of relaxation dispersion data (*Y* axis, including signs of the shift differences) versus $\Delta\varpi$ values measured directly from samples of the free and fully bound SH3 domain. Points in red are those for which the sign of $\Delta\varpi$ obtained by the method of Skrynnikov et al.[39] is correct while the blue and green colored data points refer to those for which an incorrect sign was obtained (blue) or the sign could not be established (green). Chemical shifts were obtained from dispersions recorded on the $^{13}C^{\alpha}$-labeled sample. Details are as in Figure 5.

displayed on log/log scales and where $|\Delta\varpi|$ values that vary by 2 orders of magnitude are shown.

Correlations between *signed* ^{15}N and $^{13}C^{\alpha}$ chemical shift differences measured via relaxation dispersion (signs obtained by quantification of peak positions in HSQC/HMQC spectra recorded at multiple fields) versus values obtained directly from spectra are illustrated in Figure 6, panels A (^{15}N) and B ($^{13}C^{\alpha}$), respectively. As described above for the analysis of ^{13}CO data, we have used the criteria $|\Delta\varpi| > 0.1$ ppm for selecting residues for the evaluation of the sign of the shift difference. In our experience residues for which $|\Delta\varpi| < 0.1$ ppm show very little or no shift in position with field (see inset to Figure 6B, discussed later). Of course, a cutoff of 0.1 ppm is somewhat arbitrary. For example, signs for ^{15}N $\Delta\varpi$ were incorrectly determined for Trp 3 and Asn 23 (blue) while those for $^{13}C^{\alpha}$ $\Delta\varpi$ could not be determined for Thr 5, Ala 13, Phe 20, and Asp 44 (green) and thus both possibilities for $\Delta\varpi$ are indicated in these cases; for all these residues $|\Delta\varpi| \approx 0.1$ ppm. Such ambiguities/errors are, in general, not problematic precisely because $\Delta\varpi \approx 0$. Log/log correlation plots of $|\Delta\varpi|$ are

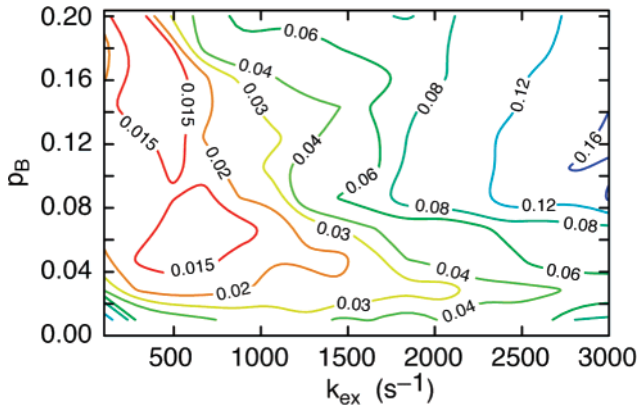

Figure 7. Contour plot showing the fractional errors (listed on the contours) that might be expected in estimated $\Delta\varpi$ values from fits of dispersion profiles recorded at 500 and 800 MHz as a function of exchange parameters, (p_B,k_{ex}). The plot was generated from fits of simulated relaxation dispersion profiles that were calculated using the same ^{15}N $\Delta\varpi$ values as measured in experiments recorded on the $^{13}C^{\alpha}$ labeled sample. Details are given in the text.

illustrated in the insets to Figure 6A,B, with color coding to indicate whether accurate/unambiguous sign information could be obtained (signs of all shift differences, irrespective of the magnitude of $|\Delta\varpi|$, are color coded). It is clear that for $|\Delta\varpi| < \sim 0.1$ ppm the accuracy of the signs becomes tenuous. It is also clear that for $|\Delta\varpi| < \sim 0.1$ there is a systematic overestimation in $|\Delta\varpi|$ from $^{13}C^{\alpha}$ dispersion data; errors of this sort are expected to be of little significance since they arise only for very small shift differences. As a final note we have also extracted ^{1}HN, ^{13}CO, and $^{13}C^{\alpha}$ chemical shifts from fits of dispersion data where (p_B,k_{ex}) were fixed to values obtained from analysis of ^{15}N dispersion profiles and there is essentially no change in chemical shift differences relative to those reported when data are fit using exchange parameters generated on a per-nucleus basis (rmsd values of 0.015, 0.004, and 0.013 ppm for ^{1}HN, ^{13}CO, and $^{13}C^{\alpha}$, respectively).

The experimental results indicate that accurate backbone chemical shifts can be obtained for the invisible bound state of the exchanging SH3 domain/peptide system under the conditions considered here where (p_B,k_{ex}) $\approx$ (7%, 250 s^{-1}) or (15%, 400 s^{-1}). A major advantage of using the experimental approach above to evaluate $\Delta\varpi$ values, rather than simulations, is that experimental imperfections are included de facto in the analysis. Nevertheless, only a limited range of parameter space can be explored for a given system. To examine a much larger range of (p_B,k_{ex}) values we have turned to computation[26] following an approach that is described in Materials and Methods. Exchange parameters ranging from $0.0\% \le p_B \le 20\%$ and $100\ s^{-1} \le k_{ex} \le 3000\ s^{-1}$, along with $\Delta\varpi$ values identical to those obtained experimentally, have been used to generate dispersion profiles that include errors (chosen from a Gaussian distribution with a width of $0.05xR_{2,eff}$, see Materials and Methods) and then analyzed in a manner identical to the experimental data. A linear correlation plot of $|\Delta\varpi_{CPMG}|$ versus $|\Delta\varpi_{Input}|$ is obtained, (see Figures 5 and 6) and a slope is calculated; the process is repeated 60 times for each (p_B,k_{ex}) with a new set of random errors chosen and an average slope and a standard deviation of the slope obtained.

Figure 7 plots the standard deviation of the slope as a function of (p_B,k_{ex}) based on an analysis of 36 simulated ^{15}N dispersion profiles that includes the range of $\Delta\varpi$ values measured

experimentally. For all exchange parameters examined the average slopes were very close to 1, between 1.06 and 0.96. However, deviations in the range of slopes from each data set can be significant for some combinations of exchange parameters, as illustrated in Figure 7. Standard deviations of 10% or more are obtained for large values of both (p_B,k_{ex}) (upper right quadrant of the plot), where dispersion profiles can become extremely large (high errors) for those residues with large $\Delta\varpi$ values; such residues (that are not "pushed" into the fast exchange regime) are important for the accurate estimation of exchange parameters that are, in turn, necessary for the extraction of correct chemical shifts. For the majority of residues the large values of k_{ex} lead to fast exchange, where $\Delta\varpi$ becomes correlated with other parameters. This has been observed experimentally on the exchanging SH3/ligand system described here where the P state is rendered invisible by adding sufficient L so that the bound form, PL, becomes the predominant state in solution. In the case that we considered, $k_{on}[L] + k_{off} \approx 2200\ s^{-1}$, $p_B \approx 5\%$ and a strong correlation between $\Delta\varpi$ and p_B is observed that precludes extraction of accurate shift values. However, for the majority of exchange parameters that normally characterize experimental systems for which high quality dispersion data can be obtained the simulations indicate that the errors are small. Profiles of the sort generated in Figure 7 based on simulations using much smaller sets of dispersion data (for example from 8 or 9 residues) indicate that errors can be larger and depend very much on the exact number of dispersion curves analyzed and the range of $\Delta\varpi$ values represented. As described in the text, in general, a robust approach for extraction of chemical shifts might be to fit dispersion data obtained from all nuclei simultaneously, so that as accurate exchange parameters as possible can be obtained. Such values of (p_B,k_{ex}) would then be used to extract chemical shift differences. In this way "accurate" values of (p_B,k_{ex}) would be used for probes in cases where dispersion from only a few residues could be quantified (perhaps $^{13}C^{\alpha}$ in some applications), increasing the quality of the extracted $\Delta\varpi$ values.

In summary, the results presented for the exchanging Abp1p SH3 domain−Ark1p peptide system establish that in principle very accurate backbone ^{15}N, ^{1}HN, $^{13}C^{\alpha}$, and ^{13}CO chemical shifts of the excited-state can be obtained by CPMG relaxation dispersion experiments. It is clear that the level of accuracy will depend on (p_B,k_{ex}) and the number of exchanging sites; however, so long as the extracted exchange parameters are not correlated with $\Delta\varpi$ values, our data indicate that accurate values of $\Delta\varpi$ can be obtained from a two-field analysis of relaxation dispersion data sets. The above analysis paves the way for the use of chemical shifts as more rigorous probes of structure for the quantification of low-populated, invisible molecular conformations.

Acknowledgment. This work was supported by a grant from the Canadian Institutes of Health Research (CIHR). D.F.H., P.V., P.L., and P.N. hold fellowships from the Danish Agency for Science, Technology and Innovation (J. No. 272-05-0232), the CIHR Training Grant on Protein Folding in Health and Disease, the Swedish Research Council and the CIHR, respectively. Valuable discussions with Dr. Dmitry Korzhnev are acknowledged.

Supporting Information Available: One pulse scheme for measuring ^{13}CO CPMG relaxation dispersion profiles. This material is available free of charge via the Internet at http://pubs.acs.org.

JA078337P